Supporting Information

Measurement of the Effect of Monovalent Cations on RNA Hairpin Stability

Jeffrey Vieregg, Wei Cheng, Carlos Bustamante, and Ignacio Tinoco, Jr.

Department of Physics, Department of Chemistry, University of California, Berkeley
Physical Biosciences Division, Lawrence Berkeley National Laboratory
Berkeley, CA 94720

S1. Thermodynamic Data

Free energies and other relevant data are tabulated (Tables S1-S6) for each of the hairpins. Number of cycles is the total number of fold/unfold trajectories analyzed. The actual number of trajectories recorded was somewhat (~10% on average) larger; trajectories showing significant drift in end-to-end extension (as measured by the difference between initial and final extension at the integration limit) were removed prior to analysis. RNA stretch work is the work required to stretch the unfolded hairpin to the upper integration bound, calculated using the wormlike chain parameters described in the main article. The uncertainty quoted for ΔG reflects both statistical and systematic effects, the latter estimated at 5.3% as described in the Experimental Section of the article.

Table S1. TAR Thermodynamic Data

Concentration (mM NaCl)	50	200	400	700	1000	100 (KCl)	400 (KCl)	1000 (KCl)
Number of Cycles	273	267	360	188	277	343	290	335
Integration Limits (pN)	8-16.5	9.5-18	12-20	11.5-19.5	11.5-19.5	10-17.5	10-18	11-19
RNA Stretch Work (kJ/mol)	23.2	24.6	26.5	26.0	26.0	24.2	24.6	25.6
ΔG (kJ/mol)	128.3 ± 9.2	154.8 ± 8.2	168.1 ± 8.9	169.6 ± 9.0	171.8 ± 9.2	135.7 ± 7.2	145.0 ± 7.7	167.4 ± 8.9

Table S2. TARdb Thermodynamic Data

Concentration (mM NaCl)	50	100	200	400	700	1000	100 (KCl)	400 (KCl)	1000 (KCl)
Number of Cycles	318	493	456	648	523	208	355	424	398
Integration Limits (pN)	12.5-17.5	13-18	14.5-19.5	15-20	15.5-20.5	16-21	13-18	14-19	15-20
RNA Stretch Work (kJ/mol)	22.8	23.2	24.5	24.9	25.3	25.7	23.2	24.1	24.9
ΔG (kJ/mol)	134.7 ± 7.1	145.0 ± 7.7	163.4 ± 8.7	180.9 ± 9.6	182.8 ± 9.7	182.8 ± 9.7	148.7 ± 7.9	158.8 ± 8.4	175.2 ± 9.3

Table S3. 30AU Thermodynamic Data

Concentration (mM NaCl)	50	100	200	400	700	1000
Number of Cycles	410	426	396	361	360	388
Integration Limits (pN)	7-11	8-13	8-13	10.5-14.5	10.5-14.5	11-15
RNA Stretch Work (kJ/mol)	21.1	24.0	24.0	26.1	26.1	59.7
ΔG (kJ/mol)	76.6 ± 4.1	109.0 ± 5.8	109.2 ± 5.8	131.0 ± 6.9	131.5 ± 7.0	146.5 ± 7.8

Table S4. AUGC Thermodynamic Data (Low Force)

Concentration (mM NaCl)	50	100	200	400	700	1000
Number of Cycles	343	302	294	313	282	311
Integration Limits (pN)	11-16	11-16	11.5-16.5	12-17	12.5-17.5	13.5-17.5
RNA Stretch Work (kJ/mol)	26.2	26.2	26.8	27.3	27.9	27.9
ΔG (kJ/mol)	144.8 ± 7.7	141.4 ± 7.5	144.5 ± 7.7	156.8 ± 8.3	159.5 ± 8.5	166.6 ± 8.8

Table S5. AUGC Thermodynamic Data (High Force)

Concentration (mM NaCl)	50	100	200	400	700	1000
Number of Cycles	343	302	294	313	282	311
Integration Limits (pN)	21-29	21-29	21.5-29.5	23-31	23.5-31.5	24-32
RNA Stretch Work (kJ/mol)	41.3	41.3	41.7	43.0	43.4	43.8
ΔG (kJ/mol)	383 ± 20	382 ± 20	384 ± 20	394 ± 21	407 ± 22	402 ± 21

Table S6. GCAU Thermodynamic Data

Concentration (mM NaCl)	50	100	200	400	700	1000
Number of Cycles	410	303	282	253	235	561
Integration Limits (pN)	10-27	9-24	10-25	8-28	10-30	11-28
RNA Stretch Work (kJ/mol)	76.5	71.0	72.9	78.2	81.6	78.2
ΔG (kJ/mol)	517 ± 28	485 ± 26	488 ± 27	534 ± 29	553 ± 30	558 ± 31

S2. Force-Extension Records

Typical force-extension trajectories for the TARdb, 30AU, AUGC, and GCAU hairpins are shown below. A typical TAR record is shown in Figure 2 of the main article. For each trajectory, unfolding (increasing force) is shown in red and folding (decreasing force) in blue.

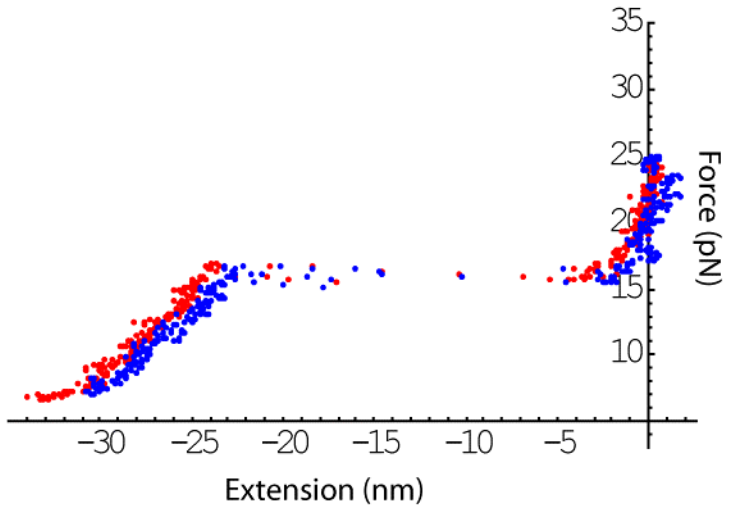

Figure S1. Typical TARdb Force-Extension Trajectory

TARdb folds and unfolds with minimal hysteresis, often "hopping" while the force is near the transition value (Figure S1). With the time resolution of our instrument, we were not able to determine whether intermediate states are occupied near equilibrium or if the hairpin is truly bistable at these forces.

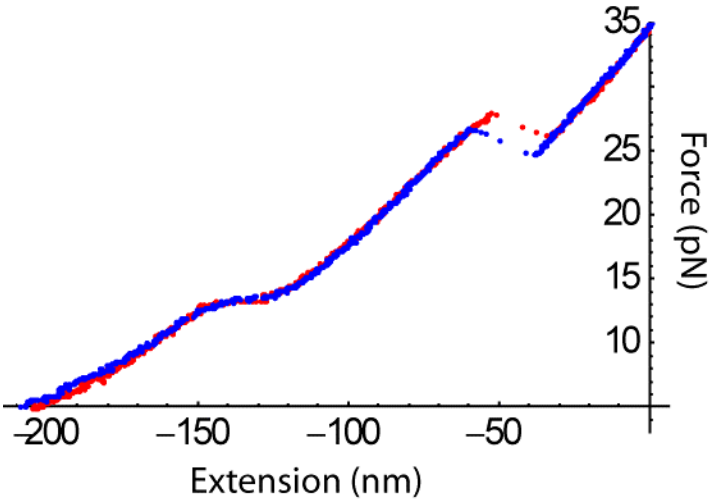

Figure S2. Typical AUGC Force-Extension Trajectory

The AUGC hairpin undergoes two transitions (Figure S2). Based on the change in extension, the low force transition corresponds to the folding/unfolding of the 30 A·U base pairs at the open end of the hairpin. This transition appears to be reversible, in that the molecular extension varies

continuously during the folding/unfolding with little change in force. The high force transition, corresponding to the unfolding of the G·C base pairs and the terminal tetraloop, displays a modest amount of hysteresis.

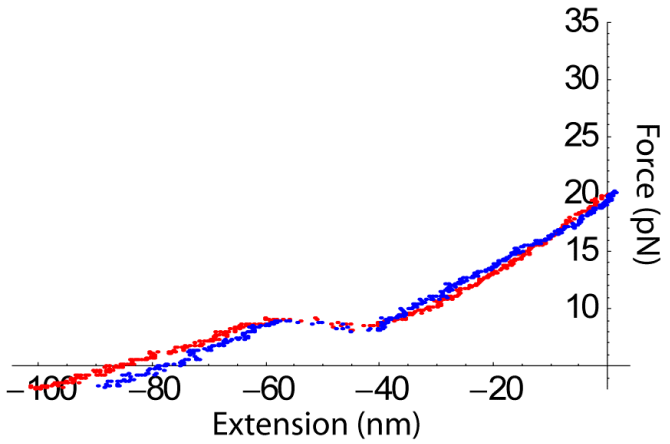

Figure S3. Typical 30AU Force-Extension Trajectory

Although the same base pairs are unfolded as during the low force transition of the AUGC hairpin, the 30AU molecule exhibits a different force-extension curve (Figure S3). There is minimal hysteresis, but folding and unfolding events are marked by a discrete change in end-to-end extension rather than a continuous transition, as well as hopping between folded and unfolded states. This apparent bistability is presumably caused by the presence of the terminal loop. Loop folding is slow compared to the opening and closing of base pairs in a helix, so the hairpin spends more time in the unfolded state. In contrast, the unfolding fork is free to diffuse along the A·U helix in AUGC, as the strongly-bound G·C pairs provide a rigid boundary without the kinetic trap of loop closure[S1].

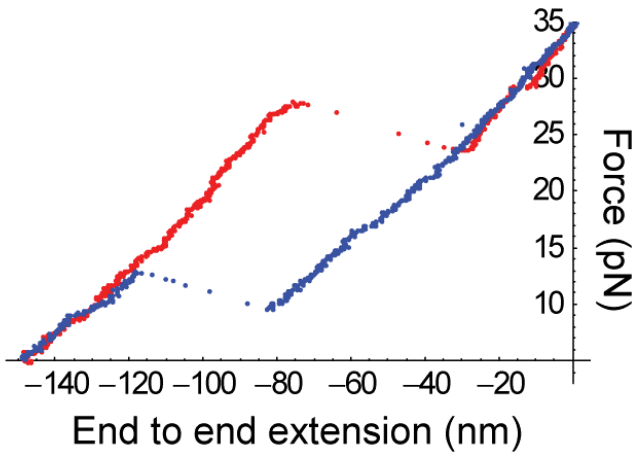

Figure S4. Typical GCAU Force-Extension Trajectory

A typical force-extension trajectory for the GCAU hairpin is shown in Figure S4. The unfolding and folding forces are widely separated, indicating significant hysteresis; this is discussed the main article.

S3. Elasticity of Single-Stranded RNA.

Figure 5 of the main article shows the data used to determine the elastic parameters of single-stranded RNA for use in the thermodynamic calculations. The errors plotted are statistical only; as mentioned in the main text, we estimated the systematic uncertainties of the force and extension measurements for the TAR and AUGC measurements to be approximately 5% and 1%, respectively. The systematic error should be similar for the P5ab hopping data, as it was obtained with the same instrument at roughly the same time. The combined data sets were fit (using nonlinear least-squares and the Levenberg-Marquardt method) allowing either the persistence or contour lengths to vary in the two-parameter wormlike chain model described in the article (Eq. 3). This resulted in values of P = 1.64 ± 0.03 nm and L = 0.633 ± 0.002 nm for the persistence and contour lengths, respectively. The reduced chi-squared values obtained were 2.38 and 2.20. Varying both the persistence and contour lengths simultaneously resulted in the

best-fit values (P = 1.26 ± 0.15 nm, L = 0.61 ± 0.01) quoted in the text, with reduced chi-squared of 1.96. Application of the F-test rejects the single-parameter fits in favor of the two-parameter fit at greater than 90% confidence level in both cases. The P5ab data show significant spread in end-to-end extension change, and as a result do not constrain the parameters well. Fitting the TAR and AUGC data alone gave similar values for the elastic parameters (P = 1.23 ± 0.21 nm, L = 0.61 ± 0.01) with an improved reduced chi-squared value of 1.21. Figure S5 shows the data and fit values. Nearly every point falls within the predicted uncertainty of the fit, with no obvious difference between low and high salt concentrations. To further examine whether we can resolve any concentration dependence of the elastic parameters, we fit the low (50 and 100 mM) and high (700 mM and 1 M) concentration data separately and compared the fit quality (reduced chi-squared of 0.51 and 0.45) to that obtained from the combined data. The resulting F-value of 1.51 confirms that the data are not statistically distinguishable. This is consistent with an earlier measurement on double-stranded DNA[S2], in which the concentration dependence saturated for NaCl concentrations above 50 mM, but appears to conflict with a measurement on poly(U)[S3]. A measurement of the force-extension curve for mixed-sequence single-stranded RNA would be ideal, but probably very difficult to obtain due to RNA's propensity to form base pairs.

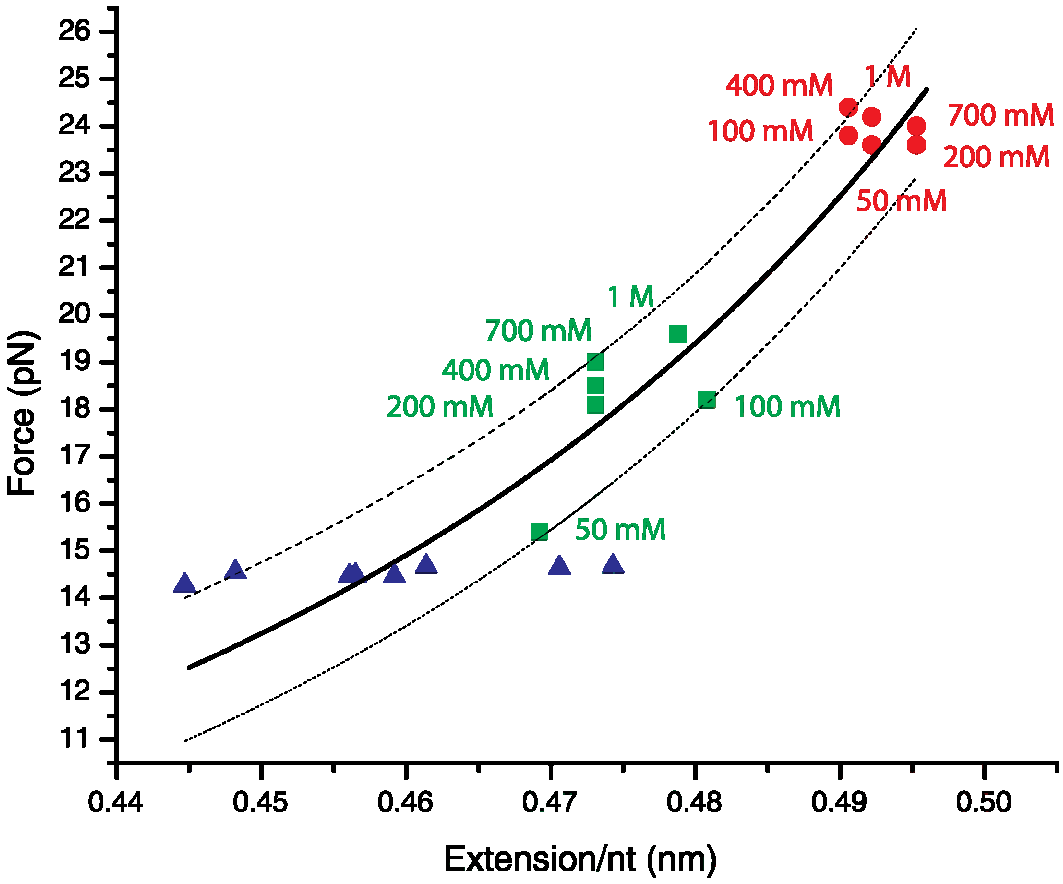

Figure S5. Data and best fit prediction for single-strand RNA elasticity. AUGC data in red, TAR data in green, and P5ab data in blue. NaCl concentration (labeled for TAR, AUGC) was 250 mM for all P5ab data. Error bars omitted for clarity. The solid line reflects the best-fit values, with 1σ prediction bands dashed.

S4. Enthalpic Stretching of RNA and RNA/DNA Handles

The wormlike chain (WLC) model described in the article (Eq. 3) considers only entropic bending elasticity of the polymer. For single and double-stranded DNA, it has been shown that the WLC model under-predicts molecular extension above ~10 pN, and that this can be accounted for by adding an additional term (stretch modulus) to allow for enthalpic stretching of the phosphate backbone[S4]. As mentioned above, few data exist for RNA elasticity. To our knowledge, the elasticity of RNA/DNA hybrids, as found in the handles in this experiment, has not been investigated at all. Seol et al. found that a stretch term was not needed to describe the

force-extension curve of poly(U). For both single and double-stranded RNA, we compared the results of fitting an extensible WLC model[S5] to those of the inextensible model. For the single strand data, the best fit elastic modulus was more than 1000 pN, and the force-extension curves predicted by the two models were indistinguishable. This is consistent with the poly(U) results, and suggests that the backbone of RNA is more difficult to stretch than that of DNA.

Considering the handle stretch work, the GCAU hairpin data should be most strongly affected by shortcomings in the inextensible model, as the force range is quite large (~ 16 pN vs. 5-8 pN for the other molecules – Tables S1-S6) and the unfolding forces are large. Qualitatively, the agreement between the inextensible model and the observed force-extension curves is somewhat worse (though still good) for these molecules than for the others. To evaluate the effects of backbone stretching, we analyzed the GCAU 100 mM NaCl data with both models and compared the results. Figure S7 shows the resulting work distributions obtained from calculating the handle stretch work using each model. The work distributions obtained with the extensible model are slightly narrower and a few kT smaller than those using the inextensible WLC. The free energy is correspondingly lower as well (470 vs. 485 kJ/mol), however, the difference is fairly small (3%). Adding the elastic modulus complicates the fitting procedure significantly; the parameters tended to be quite sensitive to the choice of initial value. Moreover, the agreement between the fit and the measured force-extension curves did not appreciably improve for the extensible model over the inextensible WLC. As a result, we decided to use the simpler inextensible model for our analysis.

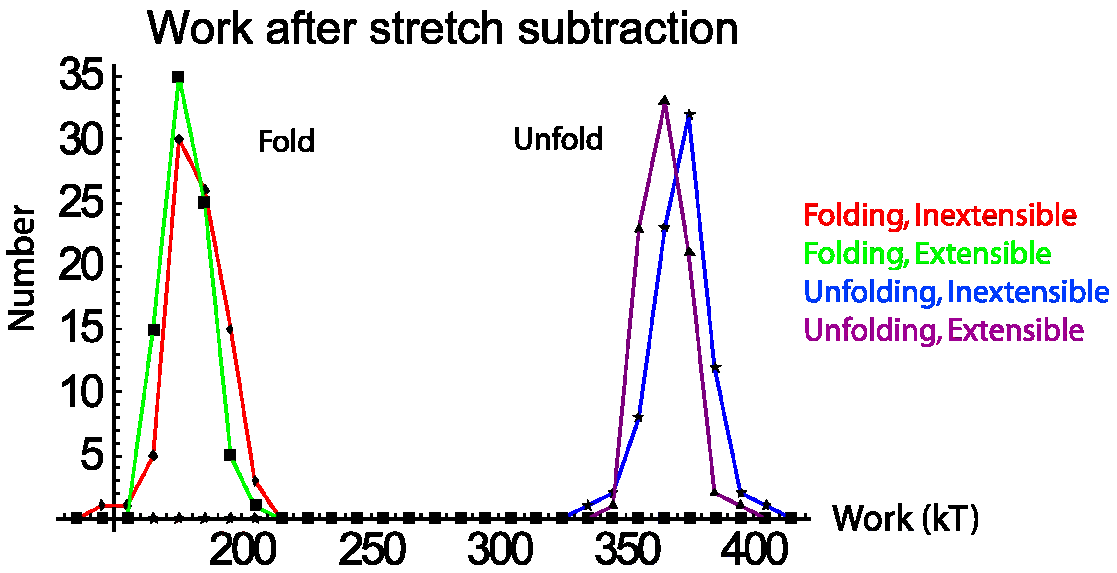

Figure S6. Folding and Unfolding Work, GCAU Hairpin in 100 mM NaCl. Distributions from inextensible model are in red (folding) and blue (unfolding). Work with extensible model shown in green (folding), purple (unfolding). Data binned at 10 kT for display only.

S5. Misfolding of the TAR Hairpin

Figure S7 shows three successive fold-unfold trajectories for the TAR hairpin in 1M NaCl. The decreasing and increasing force sections are shown in red and blue, respectively. The first trajectory shows a folding event at ~14 pN, followed by unfolding at ~20.5 pN. On the next cycle, there is no distinct folding event, rather a gradual decrease in extension (marked "Misfold" in the figure). The resulting "misfolded" state has a larger end-to-end extension than the folded state and is stable for >30 minutes at low force. When the force is subsequently increased, the molecule undergoes a folding transition (marked "Rescue"), followed by an unfolding which is indistinguishable from that of the previous cycle. This is a common phenotype for misfolding, but we also observe trajectories which do not exhibit rescue. These traces instead show only a small increase in extension as force is increased and display little hysteresis.

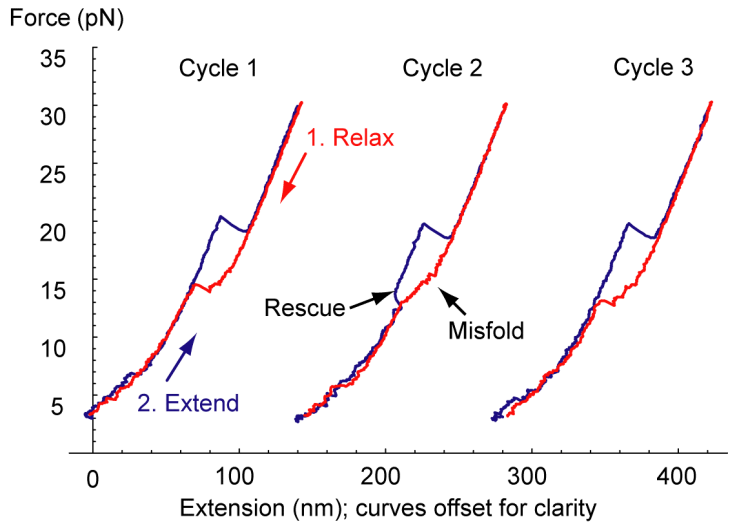

Figure S7. Misfolding Force-Extension Trajectory

In our measurement of the misfolding probability versus salt concentration (Table S7), we required trajectories to both lack a clear folding transition and to undergo either rescue or an abnormally small unfolding transition. Misfolding trajectories were easily distinguishable from proper foldings; we saw no ambiguous records. Misfolding is nearly twice as frequent in KCl as in NaCl.

Table S7. TAR Misfolding Probability vs. Salt

Concentration (mM)	50	100	200	400	700	1000
% Misfold (NaCl)	13.0 ± 1.8	11.1 ± 1.8	15.2 ± 1.7	11.3 ± 1.4	14.5 ± 2.0	14.6 ± 2.8
% Misfold (KCl)		23.4 ± 1.8		22.3 ± 2.0		22.3 ± 1.6

[S1] Vieregg, J.; Tinoco, I. *Molecular Physics* 2006, *104*, 1343-1352.
[S2] Baumann, C.G.; Smith, S.B.; Bloomfield, V.A.; Bustamante, C. *PNAS* 1997, *94*, 6185-6190.
[S3] Seol, Y; Skinner, G.M.; Visscher, K. *Phys. Rev. Lett.* 2004, *93*, 118102.
[S4] Wang, M.D.; Yin, H.; Landick, R.; Gelles, J.; Block, S.M. *Biophys. J.* 1997, *72*, 1335-1346.
[S5] Odjik, T. *Macromolecules* 1995, 28, 7016-7018.